

AD-A048 497

RAYTHEON CO WALTHAM MASS RESEARCH DIV  
HIGH DURABILITY MISSILE DOMES.(U)  
DEC 77 R GENTILMAN, E MAGUIRE, J PAPPIS  
S-2284

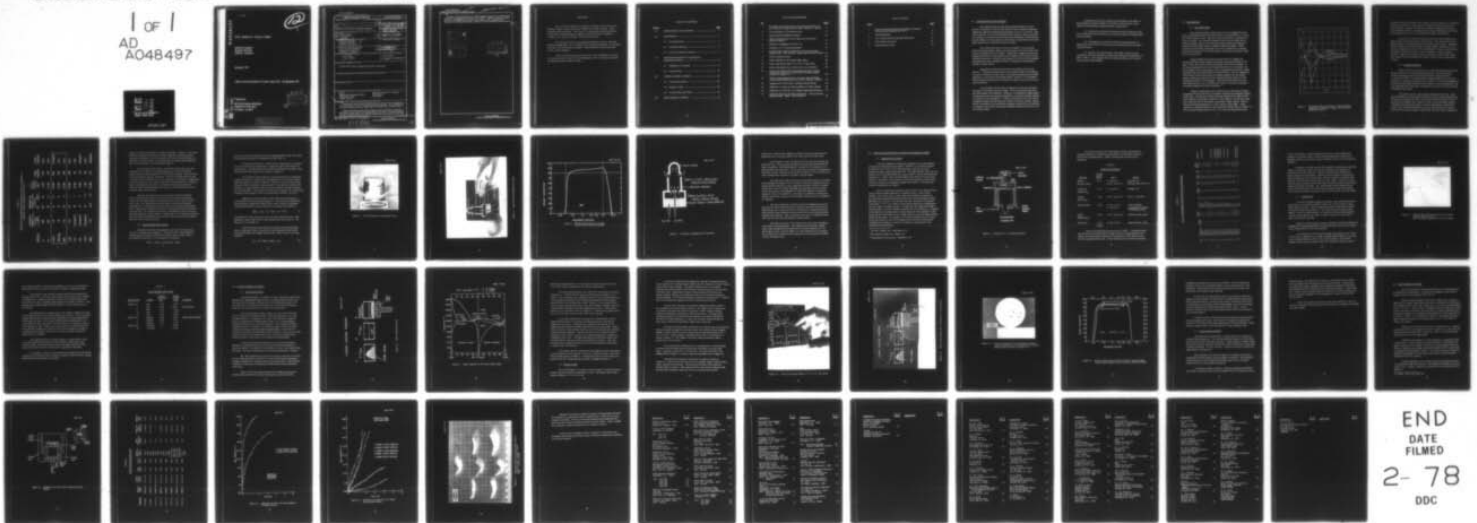
F/G 17/5

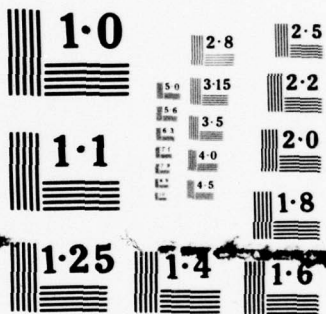
UNCLASSIFIED

N00014-76-C-0635

NL

1 of 1  
AD  
A048497





NATIONAL BUREAU OF STANDARDS  
MICROCOPY RESOLUTION TEST CHART

AD A 048497

12

HIGH DURABILITY MISSILE DOMES

Raytheon Company  
Research Division  
Waltham, MA 02154

December 1977

Interim Technical Report for Period 1 April 1976 - 30 September 1977

AD NO. \_\_\_\_\_  
DDC FILE COPY

Prepared for  
OFFICE OF NAVAL RESEARCH  
Department of the Navy  
Arlington, VA 22217

DDC  
RECEIVED  
JAN 5 1978  
D

DISTRIBUTION STATEMENT A  
Approved for public release;  
Distribution Unlimited

UNCLASSIFIED

SECURITY CLASSIFICATION OF THIS PAGE (When Data Entered)

REPORT DOCUMENTATION PAGE		READ INSTRUCTIONS BEFORE COMPLETING FORM								
1. REPORT NUMBER	2. GOVT ACCESSION NO.	3. RECIPIENT'S CATALOG NUMBER								
4. TITLE (and Subtitle) <b>6</b> HIGH DURABILITY MISSILE DOMES.		5. TYPE OF REPORT & PERIOD COVERED <b>9</b> Interim Technical Report, 1 Apr 1976-30 Sep 1977								
7. AUTHOR(s) <b>10</b> R. Gentilman, E. Maguire J. Pappis		6. PERFORMING ORG. REPORT NUMBER <b>14</b> S-2284 ✓								
9. PERFORMING ORGANIZATION NAME AND ADDRESS Raytheon Company Research Division Waltham, MA 02154 ✓		8. CONTRACT OR GRANT NUMBER(s) <b>15</b> N00014-76-C-0635 <i>new</i>								
11. CONTROLLING OFFICE NAME AND ADDRESS Office of Naval Research Department of the Navy Arlington, VA 22217		10. PROGRAM ELEMENT, PROJECT, TASK AREA & WORK UNIT NUMBERS								
14. MONITORING AGENCY NAME & ADDRESS (if different from Controlling Office) <b>12</b> H6p.		12. REPORT DATE <b>11</b> December 1977								
16. DISTRIBUTION STATEMENT (of this Report)  Approved for public release; distribution unlimited.		13. NUMBER OF PAGES 39								
17. DISTRIBUTION STATEMENT (of the abstract entered in Block 20, if different from Report)		15. SECURITY CLASS. (of this report) Unclassified								
18. SUPPLEMENTARY NOTES		15a. DECLASSIFICATION/DOWNGRADING SCHEDULE								
19. KEY WORDS (Continue on reverse side if necessary and identify by block number)										
<table border="0"> <tr> <td>Spinel</td> <td>Moisture Protective Coatings</td> </tr> <tr> <td>Magnesium Aluminum Oxide</td> <td>Hot Forging</td> </tr> <tr> <td>Magnesium Oxide</td> <td>IR Domes</td> </tr> <tr> <td>Fusion Casting</td> <td></td> </tr> </table>			Spinel	Moisture Protective Coatings	Magnesium Aluminum Oxide	Hot Forging	Magnesium Oxide	IR Domes	Fusion Casting	
Spinel	Moisture Protective Coatings									
Magnesium Aluminum Oxide	Hot Forging									
Magnesium Oxide	IR Domes									
Fusion Casting										
20. ABSTRACT (Continue on reverse side if necessary and identify by block number)										
<p>Magnesium oxide optical surfaces were protected from degradation due to moisture by any of several sputtered coatings. The coatings are of optical quality and were unaffected by rainfield tests at 256 m/sec.</p> <p>Highly transparent flat plate samples of polycrystalline magnesium aluminum oxide (spinel) were fabricated by the fusion casting technique. The best samples have a 2:1 Al<sub>2</sub>O<sub>3</sub> composition and measure more than 50 mm across and 3 mm thick.</p>										

DD FORM 1473 1 JAN 73

EDITION OF 1 NOV 65 IS OBSOLETE

UNCLASSIFIED

SECURITY CLASSIFICATION OF THIS PAGE (When Data Entered)

298 320

LB

UNCLASSIFIED

SECURITY CLASSIFICATION OF THIS PAGE(When Data Entered)

sq M

APPROXIMATELY EQUAL TO

Beams of polycrystalline and single crystal alumina-rich spinel were deformed in three-point loading at  $\approx 1750^{\circ}\text{C}$ . Applied stresses between 20 and 70 MN/m<sup>2</sup> produced up to right angle bends, suggesting the feasibility of forging flat plates of spinel into hemispherical dome shapes.

ACCESSION FOR	
NTIS	White Section <input checked="" type="checkbox"/>
DDC	Buff Section <input type="checkbox"/>
UNANNOUNCED	<input type="checkbox"/>
JUSTIFICATION.....	
BY.....	
DISTRIBUTION/AVAILABILITY CODES	
Dist.	AVAIL. and/or SPECIAL
A	

DDC  
 RECEIVED  
 JAN 5 1978  
 RECEIVED  
 D

UNCLASSIFIED

SECURITY CLASSIFICATION OF THIS PAGE(When Data Entered)

## FOREWORD

This report was prepared by Raytheon Company, Research Division, Waltham, Mass., under Contract No. N00014-76-C-0635, entitled, "High Durability Missile Domes." This work is administered under the direction of The Office of Naval Research, Material Sciences Division, Arlington, Virginia. Dr. Arthur M. Diness is the project scientist.

The work was carried out at Raytheon Research Division, Advanced Materials Department. Dr. J. Pappis is the department manager. Dr. Richard Gentilman is the principal investigator. Experimental work was performed by Mr. Edward Maguire.

This is the Interim Technical Report for Contract N00014-76-C-0635. It covers the period 1 April 1976 to 30 September 1977. The report was given the Raytheon internal number S-2284.

## TABLE OF CONTENTS

<u>Section</u>		<u>Page</u>
1.0	INTRODUCTION AND SUMMARY .....	1
2.0	BACKGROUND .....	3
2.1	The Requirement .....	3
2.2	Candidate Materials .....	5
2.3	Previous Fabrication Studies .....	7
3.0	MOISTURE PROTECTIVE COATINGS OF MAGNESIUM OXIDE .....	14
3.1	Application of Coatings .....	14
3.2	Coating Tests .....	18
4.0	FUSION CASTING OF SPINEL .....	22
4.1	Process Description .....	22
4.2	Results to Date .....	25
4.3	Current Status and Plans .....	31
5.0	HOT FORGING OF SPINEL .....	33

## LIST OF ILLUSTRATIONS

<u>No.</u>		<u>Page</u>
1	Thermally Induced Stresses at Inner and Outer Surfaces as a Function of Flight Time for Dome Stations 0° and 30°	4
2	3-Inch Diameter CVD Alumina Dome	9
3	Vapor Deposited Magnesium Oxide	10
4	Optical Transmittance of CVD MgO (Uncorrected for reflection losses.)	11
5	Schematic of Magnesia CVD Process	12
6	Schematic of r. f. Sputtering System	15
7	Polished MgO Windows Subjected to the same humidity chamber test. Left: Uncoated, Right: Silicon Nitride Coated.	19
8	Fusion Casting Process	23
9	Phase Diagram for the System MgO-Al <sub>2</sub> O <sub>3</sub> .	24
10	Fusion Cast Spinel Plate, 57 x 54 x 3.7 mm Thick.	27
11	Fusion Cast Spinel Disc, 55 mm dia x 3.0 mm Thick.	28
12	Fusion Cast Spinel Disc Photographed Between Crossed Polarizers to Reveal the Grain Structure (Same sample as shown in Figure 11.)	29
13	Optical Transmission Spectra of Fusion Cast and Single Crystal Spinel Samples(Uncorrected for reflection losses).	30
14	Apparatus for Three-Point Loading of Spinel Beams	34
15	Deflection Vs Time for Polycrystalline 2:1 Spinel Beams	36
16	Deflection Vs Time for 3. 4:1 Single Crystal Spinel Beams	37
17	Deformed Beams of Alumina-Rich Spinel. Left and Center: Single Crystal. Right: Polycrystalline.	38

## LIST OF TABLES

<u>Table</u>		<u>Page</u>
1	Infrared Transmitting Materials Rank According to Thermal Shock Resistance at 450° C	6
2	Target Materials	16
3	R. F. Sputtering Runs With MgO Substrates	17
4	Rain Erosion Test Data	21
5	Beam Deflection Runs	35

## 1.0 INTRODUCTION AND SUMMARY

The next generation of high speed infrared-guided air-to-air missiles will require a new IR dome material with increased mechanical ruggedness without sacrificing optical quality in the 3 to 5  $\mu\text{m}$  band. Magnesium fluoride, the current Sidewinder dome material, does not possess the resistance to thermal stresses (caused by aerodynamic heating during powered flight) or the resistance to rain erosion (during long-term captive flight) which will be required for future missiles.

This requirement has led to the investigation of several high durability polycrystalline oxides and of fabrication processes which could produce hemispherical dome shapes. Specifically, magnesium oxide and magnesium aluminum oxide (spinel) have emerged as the most promising candidate materials. Chemical vapor deposition (CVD) and fusion casting techniques have been developed to produce transparent polycrystalline samples of these oxides.

Materials and fabrication processes developed must be cost effective. Techniques which produce dome-shaped blanks are mandatory in order to minimize the high costs for cutting and grinding these durable materials. Even given a dome shaped blank, however, it is anticipated that finishing and polishing will represent the major portion of the cost of dome production.

A successful CVD process for magnesium oxide was developed previously on internal research funding. Both optical quality flat plates and dome shapes were deposited. However, one drawback of MgO optical components has been the gradual degradation of polished surfaces exposed to moisture in the atmosphere. A fusion casting process for fabricating transparent spinel was also explored initially on internal funding. Spinel, which is somewhat more durable than magnesium oxide and is not affected by moisture, has become the leading candidate material for future air-to-air missile domes.

Reported herein are the results of work funded by the Office of Naval Research (Contract N00014-76-C-0635) in three specific areas related to the fabrication of high durability oxide domes.

(1) It has been successfully demonstrated that magnesium oxide can be protected from moisture by any of several sputtered coatings which are also durable.

(2) Transparent and crack-free flat plate spinel samples, as large as 91 mm dia by 6.6 mm thick, have been fabricated by the fusion casting technique.

(3) Alumina-rich spinel beams, both single crystal and polycrystalline, have been deformed by three-point loading at temperatures of 1650° -1820° C. This suggests that hot forging techniques can be used to fabricate spinel dome shapes.

## 2.0 BACKGROUND

### 2.1 The Requirement

Heat seeking missiles designed for air-to-air engagements face severe operational hazards that either reduce their effectiveness or raise the overall system's cost. They are carried unprotected in exposed positions on aircraft. The infrared transparent dome can be broken during routine handling, pitted by sand and debris during takeoff and landing, or eroded by water droplet impact in flight through rain squalls. These problems are becoming increasingly severe as airspeeds are increased and as the introduction of terrain avoidance radar allows supersonic flight at very low altitudes.

Impact damage that leaves the dome intact but roughens the originally polished outer surface will degrade seeker performance in two ways. First, the minimum resolvable target size will be increased. In the current operational air-to-air missile this factor is not critical, but in the designs under consideration for the next generation missiles, seeker resolution will be severely affected by dome erosion. Second, roughening of the dome increases the amount of sunlight scattered into the seeker optics, raising the noise level in the infrared detection system and thus limiting the ability to detect targets. While these effects have not been well characterized, it is of considerable concern in current development of seekers designed for head-on approach.

Finally, immediately after missile launch, high tensile stresses are generated in the dome due to transient nonuniform aerodynamic heating of the dome. The severity of these stresses depends on the nature of the dome material (its thermal conductivity, heat capacity, and thermal expansion coefficient) and on the specific aerodynamic flight regime. Figure 1 shows the stresses generated in a dome during missile flight. These results are calculated based on a next generation missile launch at Mach 1.5 with a powered flight lasting 2.0 sec. It is seen that significant tensile

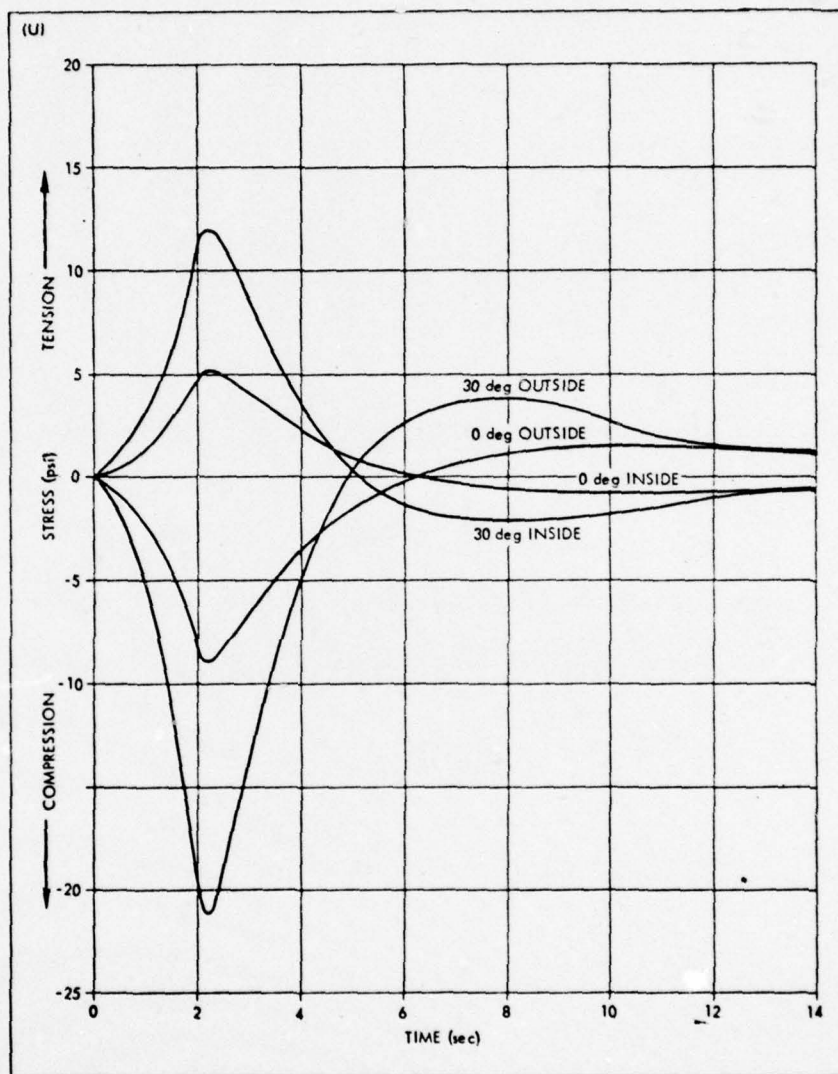


Figure 1. Thermally Induced Stresses at Inner and Outer Surfaces as a Function of Flight Time for Dome Stations 0° and 30°

stresses develop at the inside dome surface during the missile's acceleration, reaching a maximum of approximately 12,000 psi just after the end of the powered flight. However, the fracture strength of magnesium fluoride is only 10,000 psi at 450° C, the approximate average temperature of the dome during flight at the time of the maximum thermally induced stress.

Early forms of infrared missiles operated at short infrared wavelengths where fused silica domes could be used. This material has a very high resistance to thermal shock but suffers from rain erosion. Magnesium fluoride domes have provided higher strength, greater resistance to rain erosion, transparency in the 3 to 5  $\mu\text{m}$  atmospheric window, and the ability to withstand the thermal shock of current missiles in subsonic launch. However, magnesium fluoride domes are predicted to fail in either supersonic launch of current missiles or subsonic launch of the next generation designs.

## 2.2 Candidate Materials

Table 1 lists several properties of infrared transmitting materials which are pertinent to missile dome applications. The materials are ranked according to their thermal shock resistance figure-of-merit ( $= \sigma_f K / \alpha E$ ) at 450° C, the approximate average temperature of the dome at the time of maximum thermally induced stress. It is seen that magnesium fluoride has reasonable thermal shock resistance at room temperature, but it is relatively poor at the higher temperatures to which it will be subjected during high-speed flight.

The need for a new, more durable missile dome is clear. New missile designs are being compromised by the lack of a dome material with the required strength, hardness, and thermal conductivity that can be produced at an acceptable cost. However, there are several highly durable crystalline oxide materials (Table 1) that are transparent at ultraviolet, visible, and infrared wavelengths out to 5  $\mu\text{m}$  that will serve the optical needs of future seeker designs. Specifically, aluminum oxide, magnesium

TABLE 1  
 INFRARED TRANSMITTING MATERIALS RANK ACCORDING TO  
 THERMAL SHOCK RESISTANCE AT 450° C

<u>Material</u>	<u>Absorpti on Between 4-5 <math>\mu</math> in 2 mm T = 450° C</u>	<u>Resistance to Thermal Stress (<math>\sigma</math>-K/<math>\alpha</math>E) RT</u>	<u>450° C</u>	<u>R. T. Fracture Strength (psi)</u>	<u>Knoop Hardness</u>	<u>Crystal Structure</u>
Si	40%	296	60	9,000	1150	Cubic
Ge	60%	88	25	13,500	690	Cubic
Al <sub>2</sub> O <sub>3</sub>	8%	47	21	50,000	2200	Hexagonal
MgAl <sub>2</sub> O <sub>4</sub>	3%	22	11	28,000	1700	Cubic
MgO	<1%	29	8	23,000	900	Cubic
Y <sub>2</sub> O <sub>3</sub>	<1%	25	7	28,000	800	Cubic
ZnS	Transparent	26	6	15,000	356	Cubic
CdS	Transparent	19	6	8,000	130	Hexagonal
ZnSe	Transparent	23	5.5	7,500	150	Cubic
MgF <sub>2</sub>	<1%	19.4	3.2	22,000	576	Tetragonal

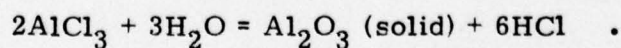
oxide, and spinel are attractive candidate materials. However, it has been difficult to fabricate dense forms of these materials by conventional hot pressing or sintering. The current state-of-the-art of sintered forms of alumina and spinel still have residual porosity that affects both target definition and sun scatter to an unacceptable degree.

Over the past several years, two alternate techniques have been developed for the production of high transparency infrared materials, namely chemical vapor deposition (CVD) and fusion casting. Each has been very successful for specific materials. The CVD technique has been used to produce polycrystalline forms of zinc selenide, zinc sulfide and magnesium oxide that represent a new state-of-the-art for these materials. Similarly, fusion casting has provided a low-cost form of calcium and strontium fluorides whose optical properties are equal to, or better than, the corresponding single crystal forms.

Both the fabrication techniques themselves and the materials under consideration are chosen to provide low cost optical components. For the present  $MgF_2$  domes, optical fabrication is not a major contribution to cost. For high durability oxide domes, however, grinding and polishing takes a much greater time and will be an important cost determinant. Replacement of present domes by a more durable material, however, could provide a very significant reduction in breakage rate and in the need for highly expensive seeker repair or replacement. It is believed, therefore, that a virtually indestructible dome would be cost effective at even several times the cost of a present dome.

### 2.3 Previous Fabrication Studies

Both aluminum oxide and magnesium oxide were fabricated previously by chemical vapor deposition. Aluminum oxide was deposited by reacting gaseous aluminum chloride with water vapor at  $1100^\circ - 1300^\circ C$  and pressures less than 5 torr according to the reaction:

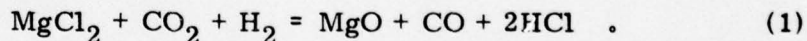


The  $\text{AlCl}_3$  vapors are produced in-line by passing chlorine gas over lumps of solid aluminum held at a temperature of  $200^\circ - 500^\circ \text{C}$ .

The aluminum chloride is volatile and is transported to the deposition zone by forced convection where it mixes and reacts with the  $\text{H}_2\text{O}$  to deposit  $\text{Al}_2\text{O}_3$ . Friable alumina was used as the deposition mandrel. Both flat plates and dome shapes were deposited (Figure 2).

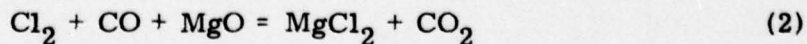
The aluminum oxide produced in this previous work is essentially completely dense but contains some intergranular porosity which scatters light and degrades its optical resolution. However, even if the last traces of porosity were eliminated, aluminum oxide is not optically isotropic and therefore, in polycrystalline form, will not be suitable for high resolution optical components. Thus, aluminum oxide domes will have to be fabricated of single crystal sapphire which is commercially available, but costly.

Magnesium oxide of excellent optical quality was fabricated in both flat plates and dome shapes (Figure 3). The material is deposited by reacting gaseous magnesium chloride with carbon dioxide and hydrogen at high temperature and reduced pressure according to the reaction:



The magnesium oxide produced by this reaction is fully dense and, when polished, is water clear with uncoated transmittance that rises to  $\sim 89$  percent at  $5 \mu\text{m}$  (Figure 4).

The CVD process used (Figure 5) involves two chemical steps. First, magnesium chloride is produced by flowing chlorine and carbon monoxide through a bed of  $\text{MgO}$  chips at  $1300^\circ - 1400^\circ \text{C}$  and 5-50 mm Hg pressure:



PBN-76-743



Figure 2. 3-Inch Diameter CVD Alumina Dome.

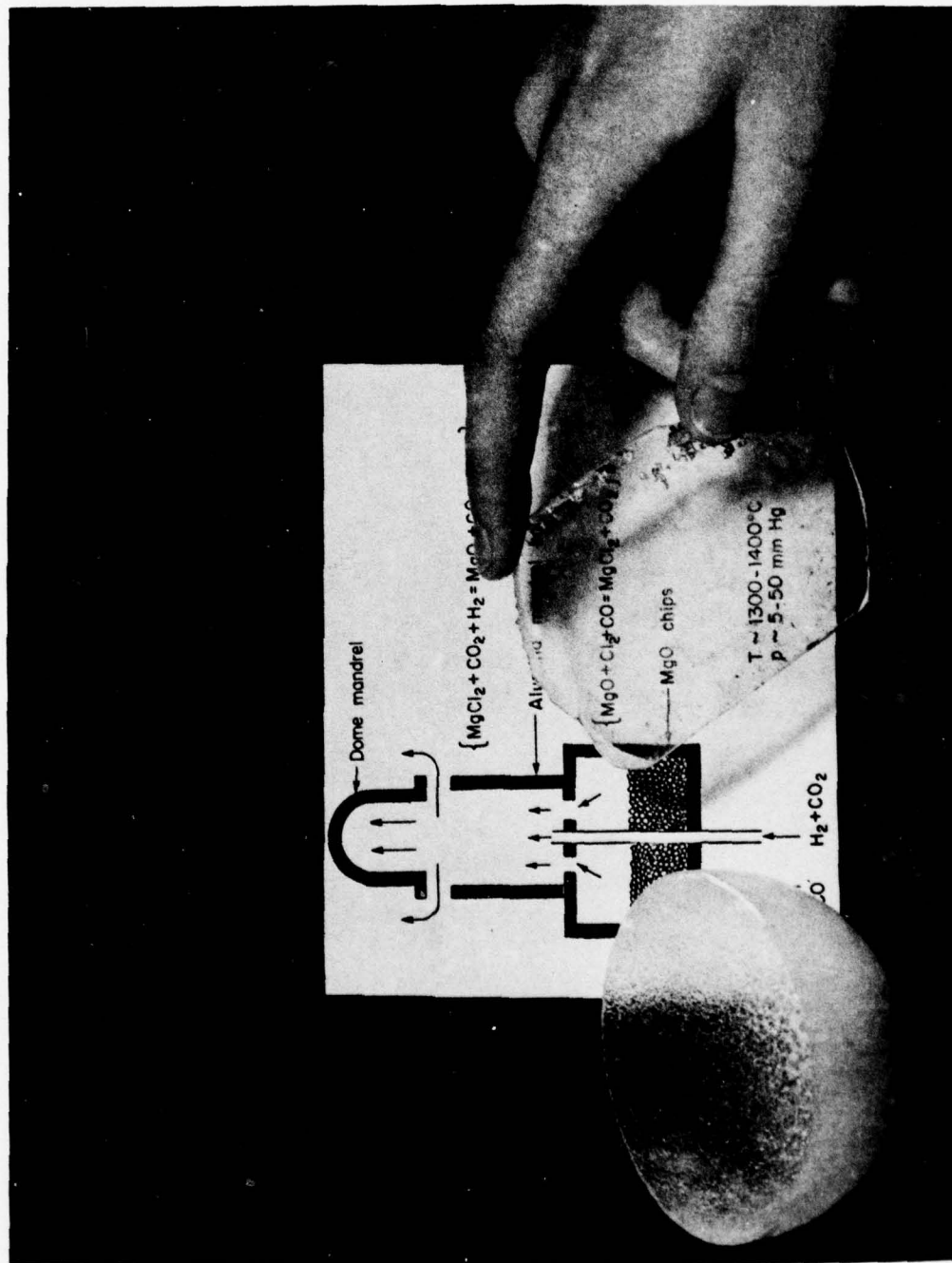


Figure 3. Vapor Deposited Magnesium Oxide.

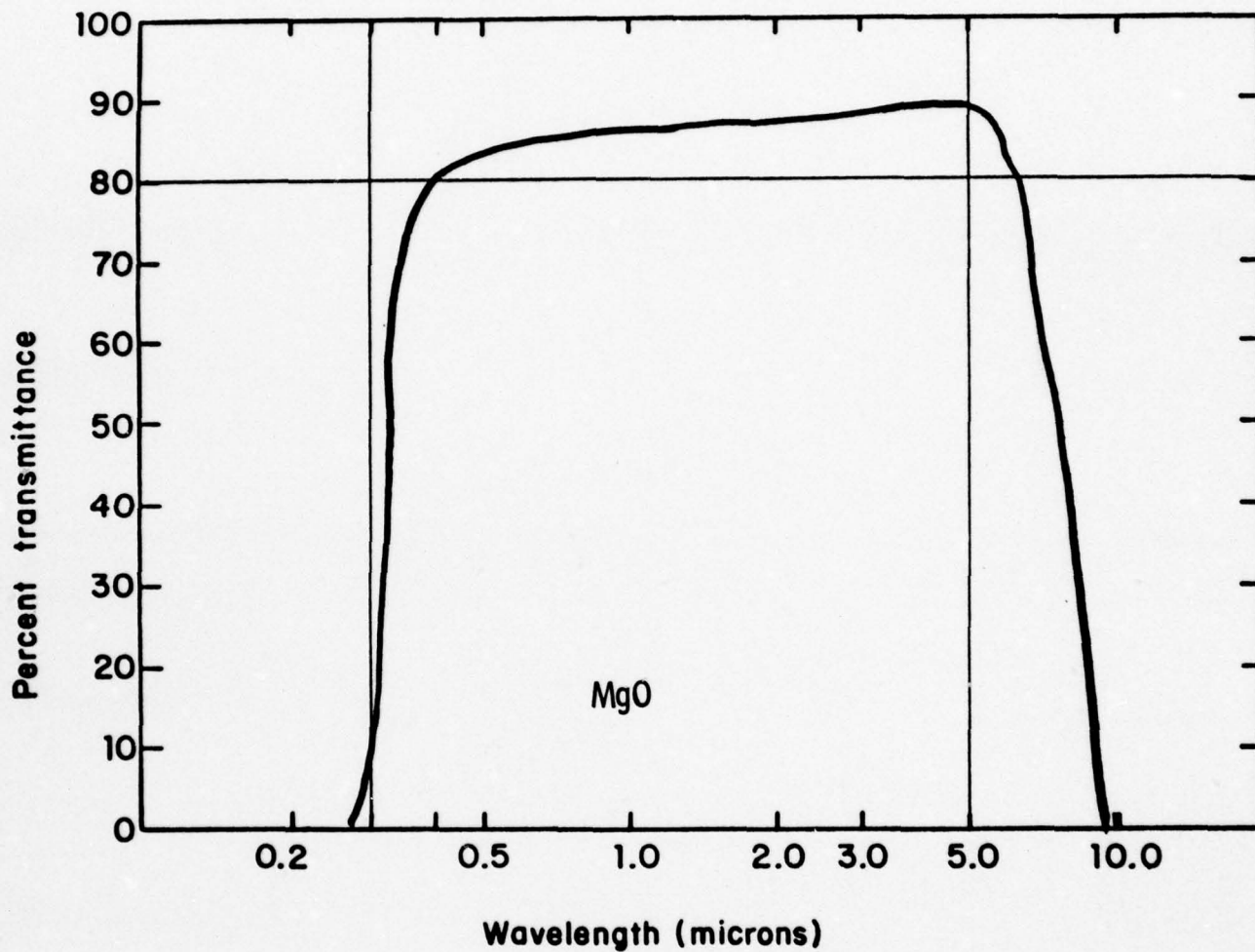


Figure 4. Optical Transmittance of CVD MgO (Uncorrected for reflection losses).

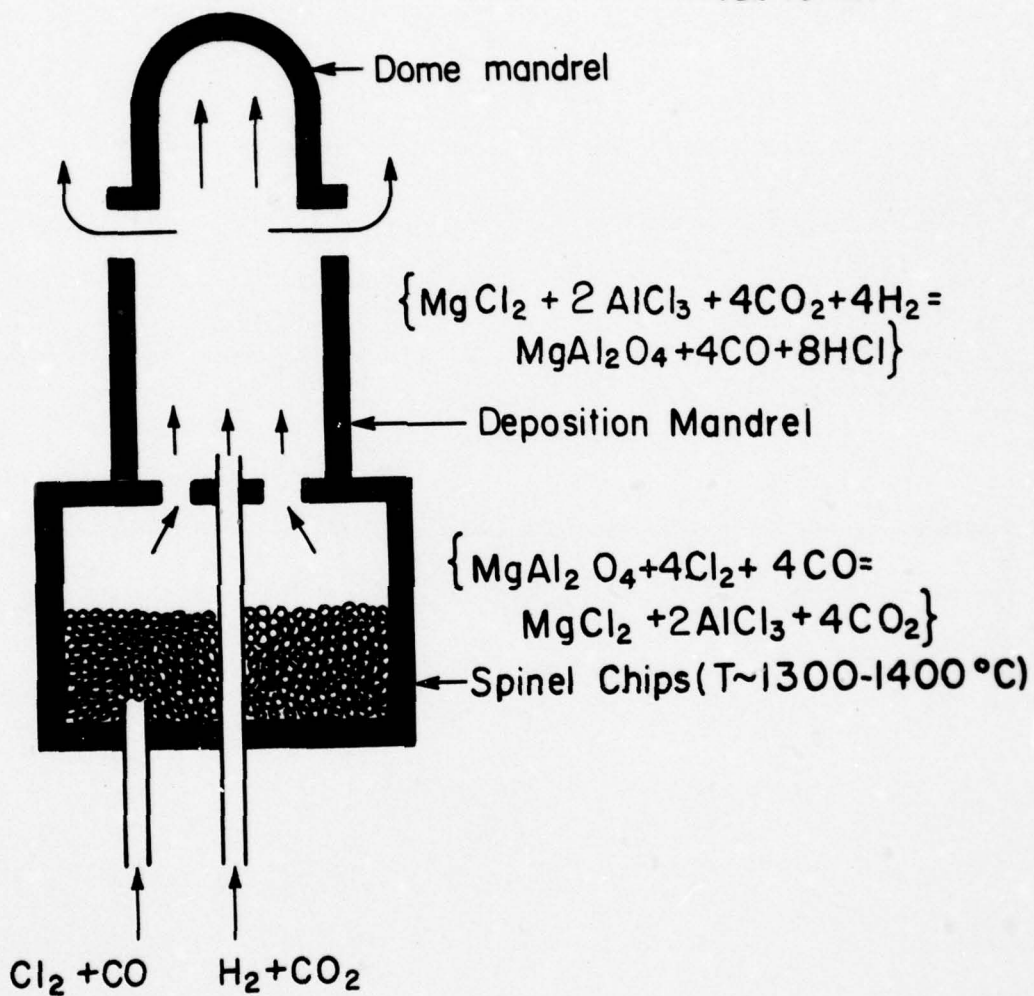


Figure 5. Schematic of Magnesia CVD Process.

Under these conditions the magnesium chloride formed is volatile and its generation rate is directly related to the input  $\text{Cl}_2$  and CO flow rates.

In the deposition zone, the  $\text{MgCl}_2$  and  $\text{CO}_2$  mix with hydrogen and additional  $\text{CO}_2$ . The  $\text{H}_2$  causes the gases to become supersaturated and the  $\text{MgO}$  is deposited. The thermodynamic driving force for reaction (1) is approximately -20 Kcal/ mole. This is sufficient to promote heterogeneous deposition of dense material on the mandrel surfaces, but not so great as to cause homogeneous nucleation of powder in the gas phase.

The magnesium oxide CVD process was demonstrated to the extent that hemispherical shapes could be produced, offering a significantly more durable IR dome than the current magnesium fluoride. However, further development of the CVD  $\text{MgO}$  technology was suspended for two reasons. First, the problem of the degradation of polished magnesia surfaces by moisture needed to be addressed. Secondly, the emphasis on fabrication studies was shifted to spinel, a more durable material and one not affected by moisture.

The vapor deposition of spinel was also investigated previously. However, the process for this three-component material was found to be significantly more complex than either the alumina or magnesia process. Some powdery spinel deposits were produced, but no free-standing dense deposits were obtained. Often, aluminum oxide and/or magnesium oxide were also obtained while attempting to deposit spinel.

Difficulties with the CVD of spinel led to the initial investigation of the fusion casting technique. This approach sacrifices the relative ease of fabricating arbitrary shapes such as domes available via CVD. Hot forging of fusion cast flat plates into dome shapes may be necessary. On the other hand, problems with composition are essentially eliminated with the casting process.

### 3.0 MOISTURE PROTECTIVE COATINGS OF MAGNESIUM OXIDE

#### 3.1 Application of Coatings

To protect magnesium oxide from degradation in the atmosphere, coatings were deposited using a Mathis<sup>\*</sup> Mark III r. f. sputtering system. It consisted of a one KW, 13.56 MHz generator coupled to the work chamber through a matching network unit. The work chamber was a 12-inch diameter by 12 inch glass walled unit atop a Welch<sup>\*\*</sup> 3102-D turbomolecular pumping unit. Water-cooled cathode targets were affixed to the top of the chamber. Substrates to be coated were positioned parallel to and directly beneath the target on an adjustable height work surface. The sputtering system is diagrammed in Figure 6.

Prior to sputtering, substrates were cleaned in an ultrasonic bath using trichloroethylene followed by a methanol rinse. In the vacuum chamber, they rested upon a copper plate whose height was adjusted to give the desired spacing between the target face and the substrate surface, generally one to six cm. The chamber was then evacuated to a pressure of less than  $5 \times 10^{-5}$  torr before introducing the high purity working gases such as oxygen, nitrogen or argon. The gas flow was regulated through a metering valve to provide chamber pressures of 5 to 50 millitorr. Pressure in the chamber was determined by a high sensitivity Pirani gauge.<sup>#</sup> A glow discharge was established and the voltage adjusted to give the desired power density at the target. The duration of runs was ordinarily 24 hrs or less. At the conclusion of a run, the discharge was turned off and the system backfilled to atmospheric pressure to enable the coated pieces to be removed from the chamber.

---

\* The R. D. Mathis Co., Long Beach, CA.

\*\* The Welch Scientific Co., Skokie, IL.

# Consolidated Vacuum Corp., Rochester, NY.

PBN-77-485

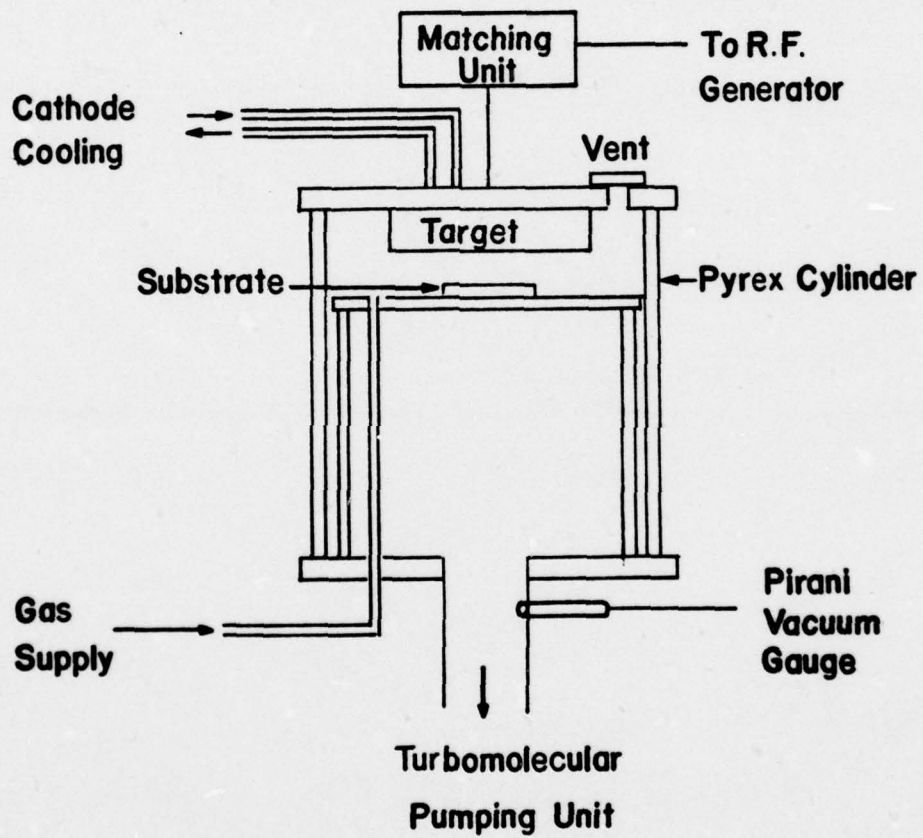


Figure 6. Schematic of r. f. Sputtering System

The targets employed were flat plates of dense polycrystalline materials bonded to an aluminum backing plate by a thermally conductive electrically insulating epoxy. Table 2 includes data on these source materials.

TABLE 2  
TARGET MATERIALS

<u>Material</u>	<u>X-Ray Density (g/cc)</u>	<u>Size</u>	<u>Source</u>
Mullite ( $3\text{Al}_2\text{O}_3 \cdot 2\text{SiO}_2$ )	3.26	3" dia x 3/8" 2-5/8" dia x 1/4"	Haselden Co. McDanel Refr. Porc. Co.
Forsterite ( $2\text{MgO} \cdot \text{SiO}_2$ )	3.22	3" dia x 1/4"	Haselden Co.
Steatite ( $\text{MgO} \cdot \text{SiO}_2$ )	3.20	2-3/8" dia x 1/8"	3M Co., Code 645
Beryllia (BeO)	3.01	2" x 2" x 1/8" 6" dia x 1/4"	Brush-Wellman Consolidated Ceramics & Metallizing Corp.
Spinel ( $\text{MgO} \cdot \text{Al}_2\text{O}_3$ )	3.58	2-5/8" dia x 3/8"	Raytheon (fusion cast)
Silicon (Si) ( $\text{Si}_3\text{N}_4$ )	3.18	6" dia x 3/16"	Materials Res. Corp.

Data on the sputtering runs are given in Table 3. Coating thickness was determined by attributing any weight increase during deposition to the deposit and calculating the appropriate thickness for a fully dense coating over the exposed surface area. X-ray densities given in Table 2 were used

TABLE 3

R. F. SPUTTERING RUNS WITH MgO SUBSTRATES

Run	Sample Code	No. of Samples	Size of Samples (in.)	Coating	Atm.	Pressure (mtorr)	Time (hr)	Power (KW)	Gap (cm)	Film Thickness ( $\mu\text{m}$ )	Comments
5	23420-98	1	1 x 1	Mullite	O <sub>2</sub>	15	8.0	0.24	---	1.20	Film flaked off
28	24630-20	1	1 x 1	Mullite	O <sub>2</sub>	30	7.0	0.20	---	---	---
6	23420-98	1	1 x 1	Forsterite	O <sub>2</sub>	15	8.0	0.24	---	1.10	---
7	23420-100	1	1 x 1	Steatite	O <sub>2</sub>	15	39.5	0.25	---	8.33	---
62	24630-39	3	0.5 x 1.5	Steatite	O <sub>2</sub>	15	25.0	0.18	3.3	2.9-3.2	---
63	24630-39	3	0.5 x 1.5	Steatite	O <sub>2</sub>	15	8.0	0.16	3.3	0.9-1.0	---
16	24630-10	2	1 x 1	Spinel	O <sub>2</sub>	50	23.0	0.17	---	---	Film flaked off
17	24630-10	2	1 x 1	Spinel	O <sub>2</sub>	10	6.5	0.22	---	---	---
18	24630-10	2	1 x 1	Spinel	O <sub>2</sub>	10	6.5	0.22	---	---	Film flaked off
19	24630-12	3	0.5 x 1.5	Spinel	O <sub>2</sub>	10	6.5	0.22	---	0.7-1.5	Film flaked off
20	24630-13	2	1 x 1	Spinel	O <sub>2</sub>	10	6.25	0.22	---	---	Film flaked off
21	24630-14	2	0.5 x 1.5	Spinel	O <sub>2</sub>	10	8.0	0.22	---	---	Film flaked off
22	24630-17	2	1 x 1	Spinel	O <sub>2</sub>	10	7.0	0.22	---	---	---
33	24630-23	1	1 x 1	Spinel	O <sub>2</sub>	40	8.0	0.18	---	2.09	Poor adherence
34	24630-23	1	1 x 1	Spinel	O <sub>2</sub>	40	8.0	0.18	---	1.58	---
43	24630-29	1	1 x 1	Spinel	O <sub>2</sub>	30	6.0	0.10	6.0	2.20	Film flaked off
23	24630-18	1	1 x 1	BeO	O <sub>2</sub>	25	6.5	0.16	---	---	---
30	24630-21	2	0.5 x 1.5	BeO	O <sub>2</sub>	25	7.0	0.17	---	2.6-2.7	---
31	24630-21	2	0.5 x 1.5	BeO	O <sub>2</sub>	25	17.0	0.17	---	7.9-8.8	---
59	24630-37	7	0.5 x 1.5	BeO	O <sub>2</sub>	10	---	---	3.5	1.3-3.8	Excellent films
--	-----	-	1 x 1	Si <sub>3</sub> N <sub>4</sub>	N <sub>2</sub>	10	2-6	0.19	---	1.6-5.0	Typical conditions

in these calculations. Infrared reflectance spectra of the coatings were measured on a Perkin-Elmer, Model 457 spectrophotometer fitted with a specular reflectance accessory using an aluminum mirror as the 100 percent standard.

In general, optically smooth and transparent coatings were achieved using r. f. sputtering. Spinel and beryllia coatings were crystalline as determined by X-ray diffraction, while the coatings of the silicates and silicon nitride were amorphous. Adherence was a problem with spinel and less frequently for other coating types, with the exception of forsterite and steatite which showed excellent adhesion in all cases. In general, it was found that the best adhesion was achieved at the lowest pressure which would sustain the plasma discharge. The optimum gap between target and substrate was determined to be the minimum possible provided the substrate was not within the plasma dark space which occurs directly below the target.

### 3.2 Coating Tests

A number of polished magnesia samples, both coated and uncoated, were tested in a controlled humidity chamber for 72-78 hrs at 65° C and 100% relative humidity. These conditions caused the unprotected surfaces to become clouded and translucent. All coated surfaces remained clear. Figure 7 shows two MgO samples, one coated on both sides with sputtered silicon nitride (right) and the other uncoated, which were tested side by side in the humidity chamber.

Based on visual inspection and by comparison of infrared reflectance spectra of the coatings taken before and after the test, there was no indication of deterioration of any of the coatings.

As a further test of the coating strength and adherence, ten 0.5 by 1.5 by 3/16 in. samples of Avco MgO, weighing approximately 8.1 g, were sent to Wright-Patterson AFB for rain erosion testing. Two of these samples were uncoated controls, three were coated with steatite, and five

PBN-77-718

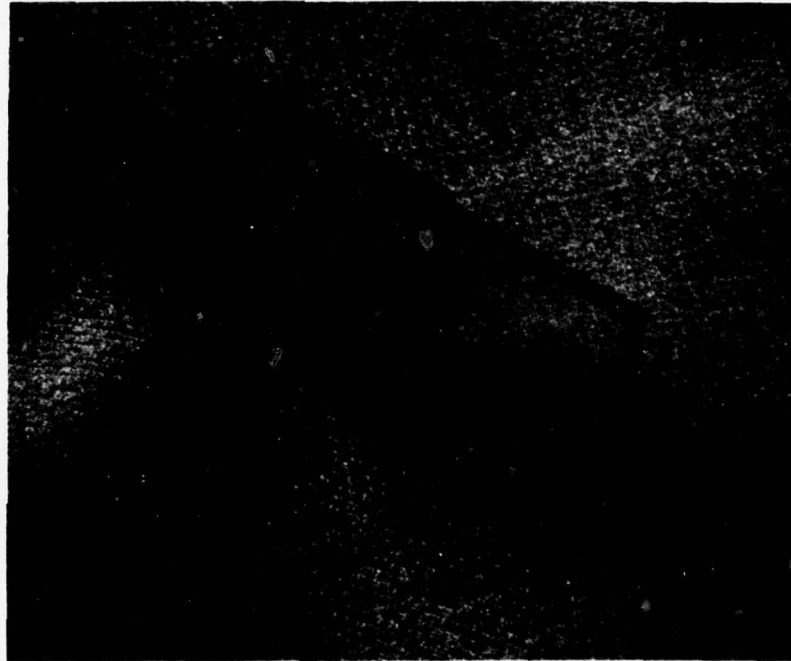


Figure 7. Polished MgO Windows Subjected to the Same Humidity Chamber Test.  
Left: Uncoated, Right: Silicon Nitride Coated

were coated with BeO. All were run through a 1.0 in. per hr rainfield for 20 minutes at 256 m/sec (575 mph) with a 90 degree impingement angle.

The surfaces of the uncoated samples showed some degradation, although not severe. All of the coated surfaces were intact with no changes in transparency. Infrared reflectance spectra were identical before and after this test. Data, including weight changes, are shown in Table 4. Two samples were chipped slightly during shipment or when clamped into the test fixture.

Discounting the two samples which were slightly chipped, the maximum weight loss for the six coated samples was 1.58 mg. The two uncoated samples showed some moderate surface degradation and had weight losses of 12.8 and 14.9 mg. It is not known whether surface degradation of uncoated MgO was due to the effects of liquid impact or the moisture inherent to the testing, or both. While it has not been proven conclusively that the thin sputtered coatings give improved rain erosion resistance for MgO, it is clear that the coatings remain intact under the rainfield conditions to which they were exposed.

As an additional test of coating integrity, a representative selection of the samples were subjected to the humidity chamber after rain erosion testing. The coated front surfaces were again unaffected while the uncoated bottom and side surfaces were significantly degraded.

In summary, it has been demonstrated that magnesium oxide optical surfaces can be protected from moisture by sputtered optical quality coatings which have also been shown to be durable.

TABLE 4

RAIN EROSION TEST DATA

<u>Sample Code</u>	<u>Coating</u>	<u>Coating Thickness (<math>\mu\text{m}</math>)</u>	<u>Weight Change (mg)</u>	<u>Comments</u>
24630-37-6	BeO	1.69	-0.88	
-7	BeO	1.38	-110.0	Edge chipped
-8	BeO	1.27	+0.08	
-9	BeO	1.32	-0.64	
-10	BeO	1.63	-0.22	
24630-39-1	Steatite	2.95	-12.38	Edge chipped slightly
-2	Steatite	2.86	-0.12	
-3	Steatite	3.18	-1.58	
24630-59-9	Uncoated	----	-12.80	
-10	Uncoated	----	-14.92	

## 4.0 FUSION CASTING OF SPINEL

### 4.1 Process Description

The starting charge is a mixture of Linde C aluminum oxide (Union Carbide) and reagent grade MgO (Fisher) of a predetermined molar ratio. The powders are weighed, blended, and then isostatically pressed. For the early runs, the charge was pre-fired in air to form the spinel phase; however, this step has since been found to be unnecessary.

The pressed powder charge is placed in a thin-wall mold made from 0.13 mm thick molybdenum foil. Molds measuring 9 to 15 cm dia. by approximately 3 cm high have been used. The material is heated to above its melting point of approximately 2100° C in a vertical graphite resistance furnace with a cylindrical element. After holding the melt at temperature for 2 to 4 hours, it is solidified in place. Due to the large volume contraction upon solidification (approximately 14 percent), it is necessary to solidify unidirectionally from the bottom to the top of the mold. If this is not done, the solidification will be initiated at random growth sites and result in macroscopic voids between individual grains.

To effect unidirectional solidification, a vertical temperature gradient is maintained within the melt while the furnace temperature is slowly decreased. The gradient is established by a heat sink situated below the mold. The fusion casting process is shown schematically in Figure 8.

The high temperatures required for casting of spinel do not permit the use of thermocouples to monitor or control the process temperature. Instead, temperature is measured with an optical pyrometer, and the slow cooldown is achieved by controlling the furnace power with an automatic clock drive.

Figure 9 shows the phase diagram for the MgO-Al<sub>2</sub>O<sub>3</sub> system. Although the positions of the solidus and liquidus lines have not been

# FUSION CASTING PROCESS

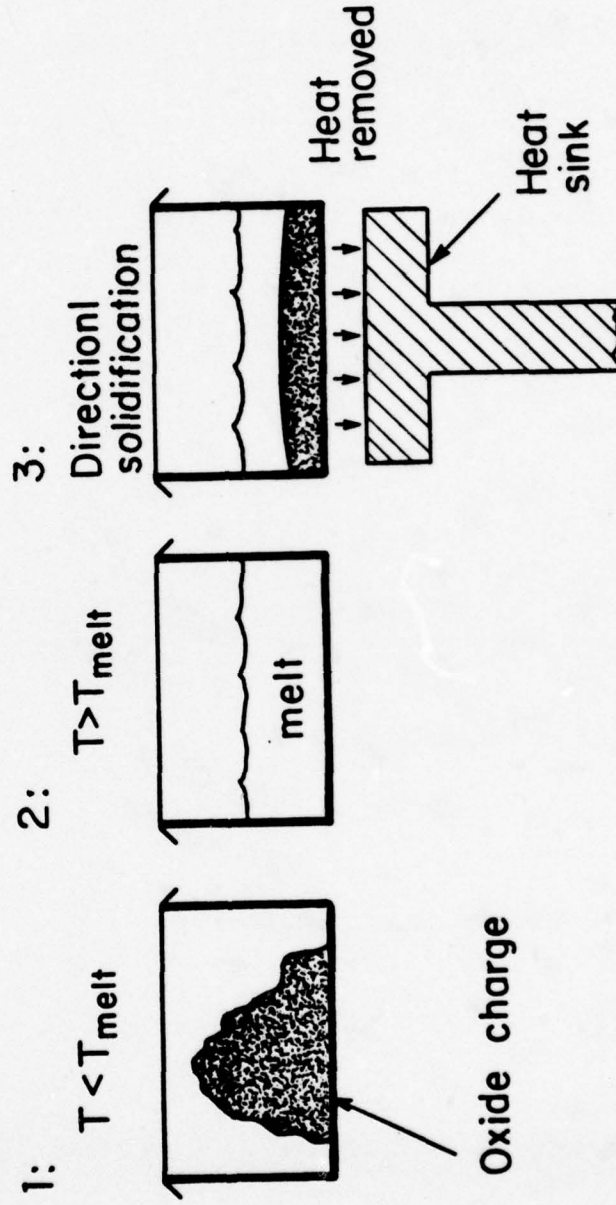


Figure 8. Fusion Casting Process.

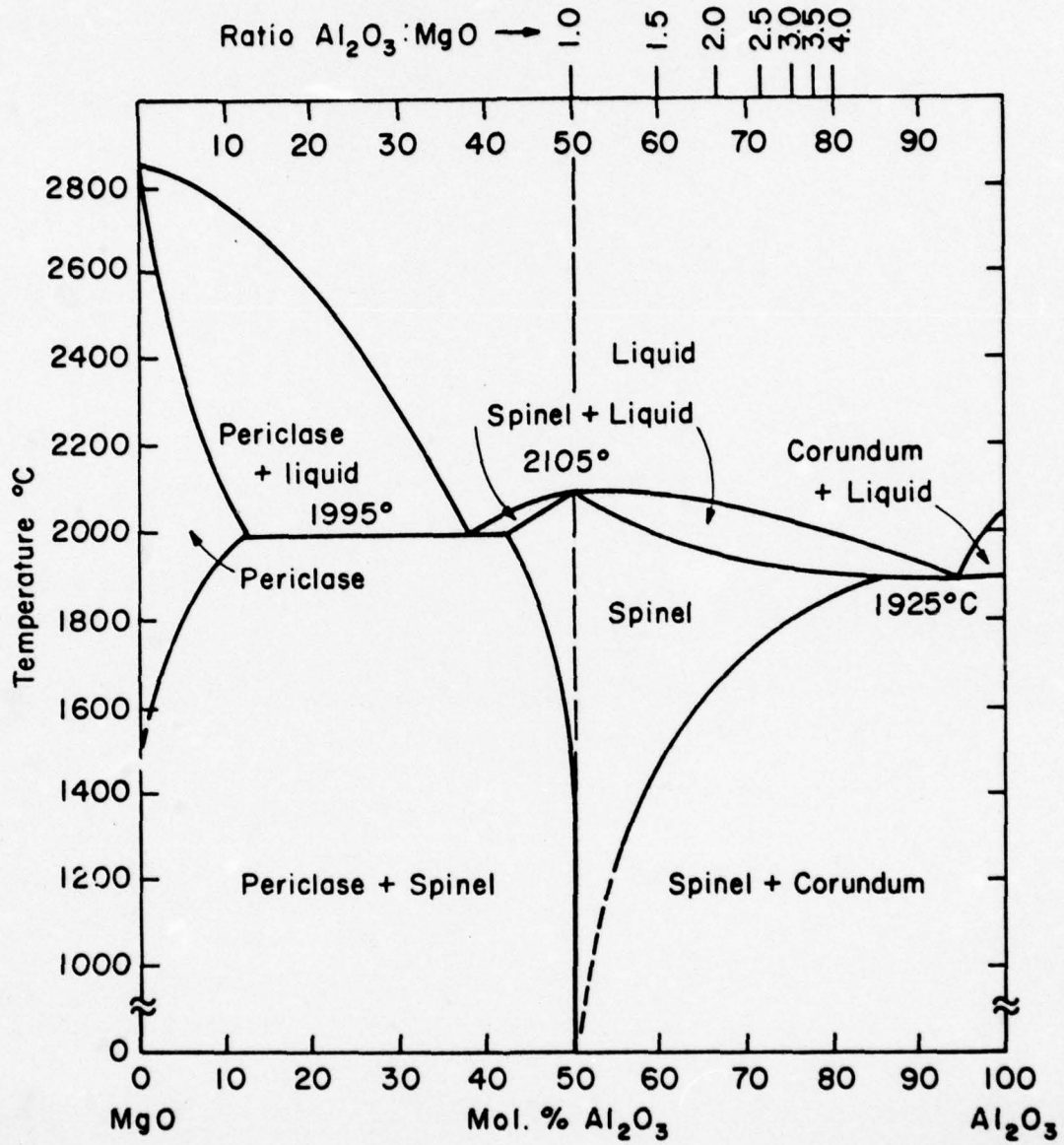


Figure 9. Phase Diagram for the System MgO-Al<sub>2</sub>O<sub>3</sub>.

determined unambiguously, it is seen that the spinel structure can exist over a wide range of compositions at elevated temperatures.

The initial casting studies were made with stoichiometric starting charges, i. e., 50 mole percent  $\text{Al}_2\text{O}_3$  and 50 mole percent  $\text{MgO}$ , or 1:1 spinel. This composition was originally chosen to avoid potential problems of second phase precipitation and compositional gradients which might be expected with a non-stoichiometric melt. However, even though stoichiometric starting charges were used, a few percent  $\text{MgO}$  invariably vaporizes at temperature making the castings slightly alumina-rich. Subsequently, alumina-rich compositions were investigated. A starting  $\text{Al}_2\text{O}_3$ : $\text{MgO}$  molar ratio of 2:1 has been used for most of the recent castings.

At the high temperatures necessary for melting spinel, certain undesirable reactions occur between molybdenum and the melt and the graphite furnace parts. Molybdenum is oxidized by the few percent of magnesium oxide which invariably vaporizes from the spinel melt. Molybdenum oxides are formed which dissolve in the melt and leave the resulting casting somewhat darkened. This discoloration can be reduced by post-annealing in air at  $1600^\circ\text{C}$ ; however, the annealed material is usually not completely water clear. The  $\text{MgO}$  vaporization rate has been reduced but not eliminated by casting in helium at atmospheric pressure. Also, pre-cleaning of the molybdenum molds with a household bleach has been found to minimize the discoloration.

The reaction between molybdenum and graphite has been minimized by using tantalum foil as a spacer. However, a eutectic exists in the molybdenum-carbon system at  $2200^\circ\text{C}$ . This has been found to be the upper temperature limit for using molybdenum molds in graphite furnaces.

#### 4.2 Results to Date

The best castings of 1:1 spinel contained regions of excellent optical quality material bounded by solidification voids. The largest water-clear sample measured  $\sim 2 \times 2 \times 0.3$  cm.

Two major problems which plagued the casting of nominally stoichiometric spinel were cracking during cooldown and the existence of bubble regions at the bottom of the castings. This latter problem is due to incomplete melting of the spinel charge at the bottom of the mold because of its proximity to the heat sink. Reducing the amount of heat extracted by the heat sink allows complete melting, but solidification then occurs randomly instead of unidirectionally. The furnace temperature cannot be increased above  $\sim 2200^\circ\text{C}$  due to the molybdenum-graphite eutectic as discussed previously.

The use of 2:1 alumina-rich starting charges has greatly reduced the cracking and residual bubble problems. The slightly lower melting point of alumina-rich spinel (see Figure 9) appears to allow complete melting within the temperature limitations of the present setup. Cracking during cooldown has also been reduced because alumina-rich spinel compositions are ductile at high temperatures. Thus, the stresses created during cooldown can be relieved by deformation rather than by fracture.

Several defect-free plates of alumina-rich material have been produced. These are totally transparent and water-clear with excellent optical imaging quality. Figure 10 shows one such sample with overall dimensions of  $57 \times 54 \times 3.7$  mm. Another sample, measuring 55 mm dia  $\times$  3.0 mm thick, is shown in Figure 11. The largest crack-free casting produced to date is 91 mm dia  $\times$  6.6 mm thick.

Due to directional solidification, the castings have a columnar grain structure with individual grains running from the bottom to the top of the ingot. Typically, grains are 2-5 mm across. The grain structure of the polished disc in Figure 11 is shown using crossed-polarizers in Figure 12.

The optical transmittance of alumina-rich spinel is shown in Figure 13. Also shown is the spectrum of Czochralski single crystal stoichiometric spinel (Union Carbide). The spectra are plotted uncorrected for fresnel reflection losses. Both materials show near intrinsic behavior with the electronic absorption edge near  $0.3 \mu\text{m}$  in the ultraviolet and the

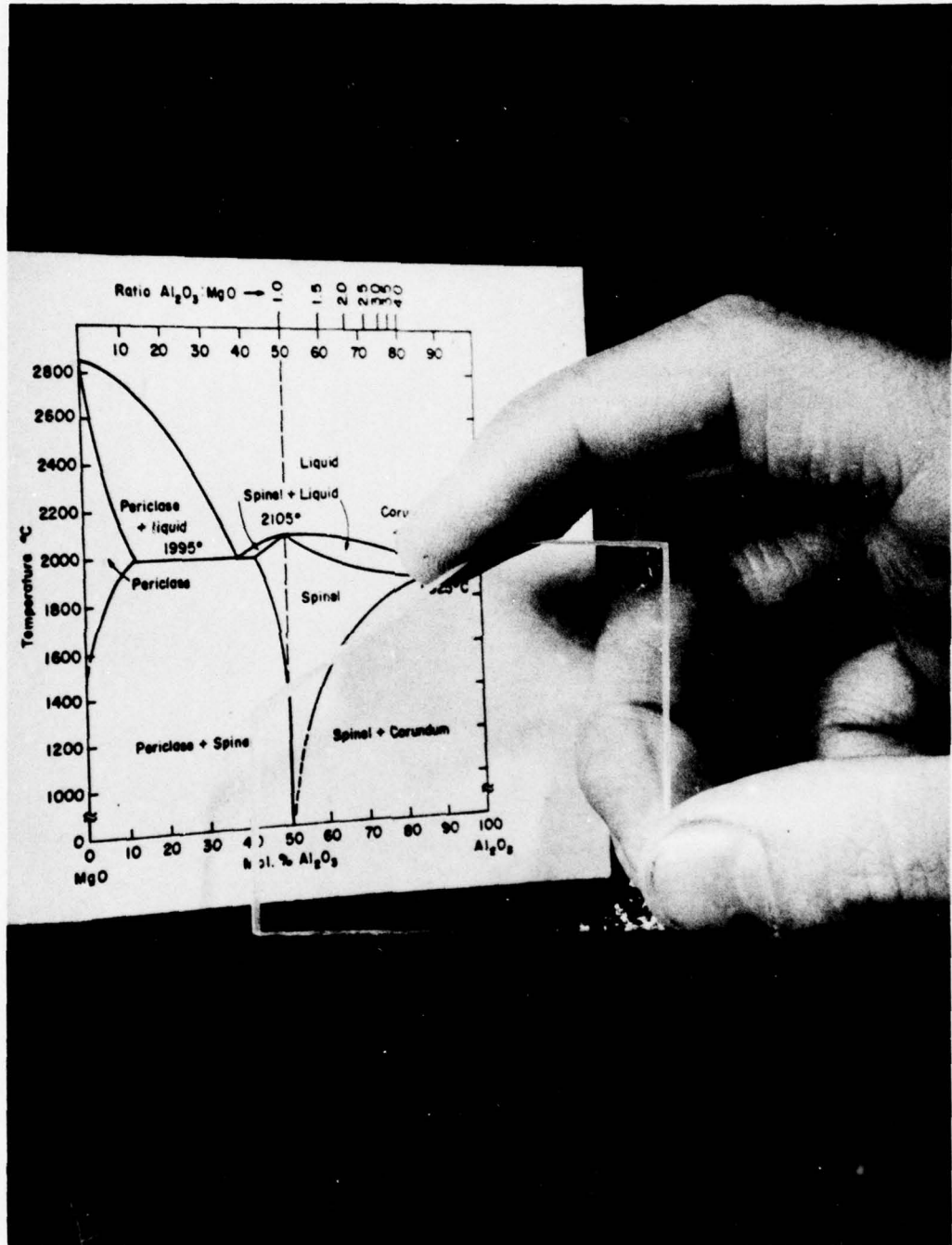


Figure 10. Fusion Cast Spinel Plate, 57 × 54 × 3.7 mm Thick.

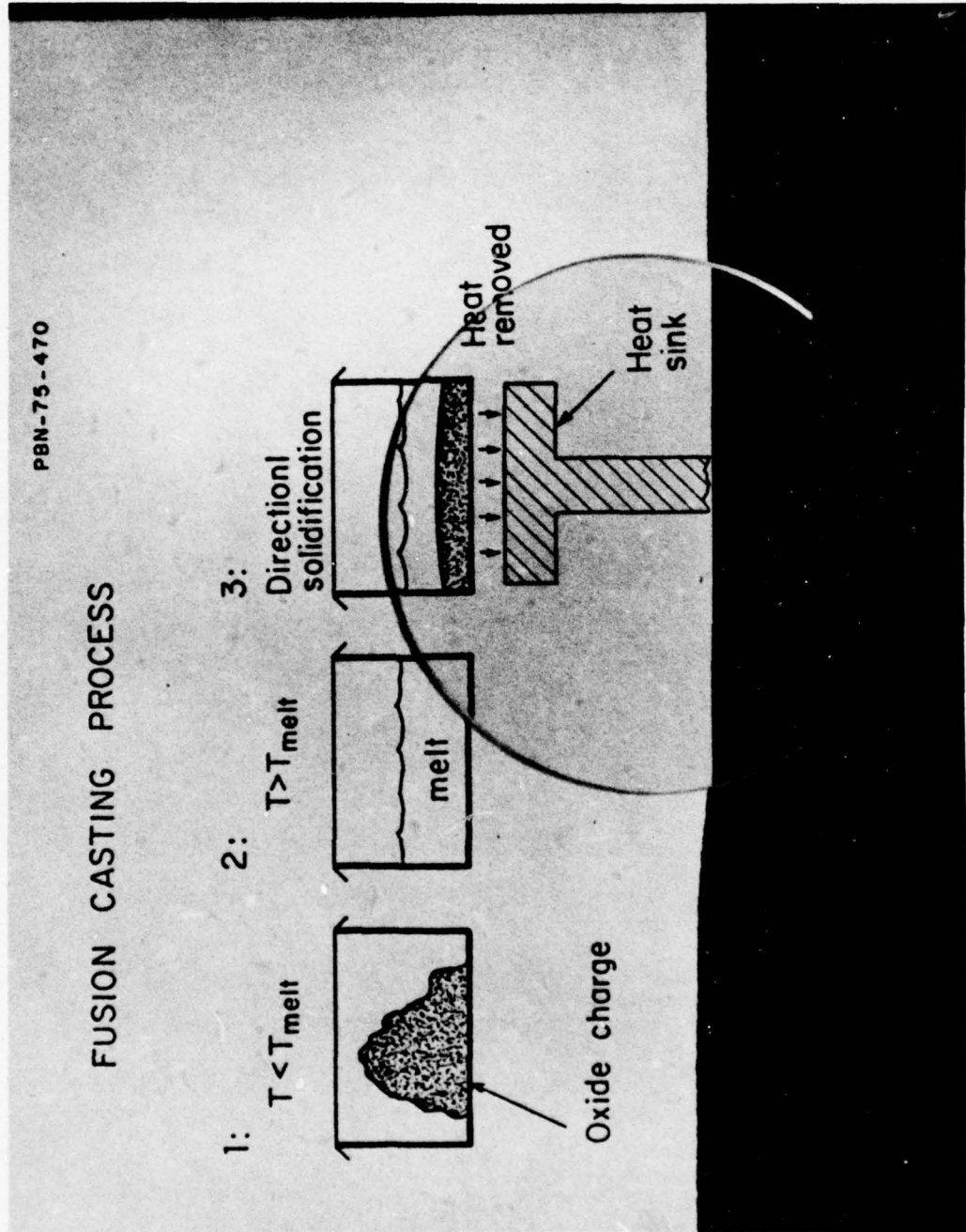


Figure 11. Fusion Cast Spinel Disc, 55 mm dia X 3.0 mm Thick.

PBN-77-720

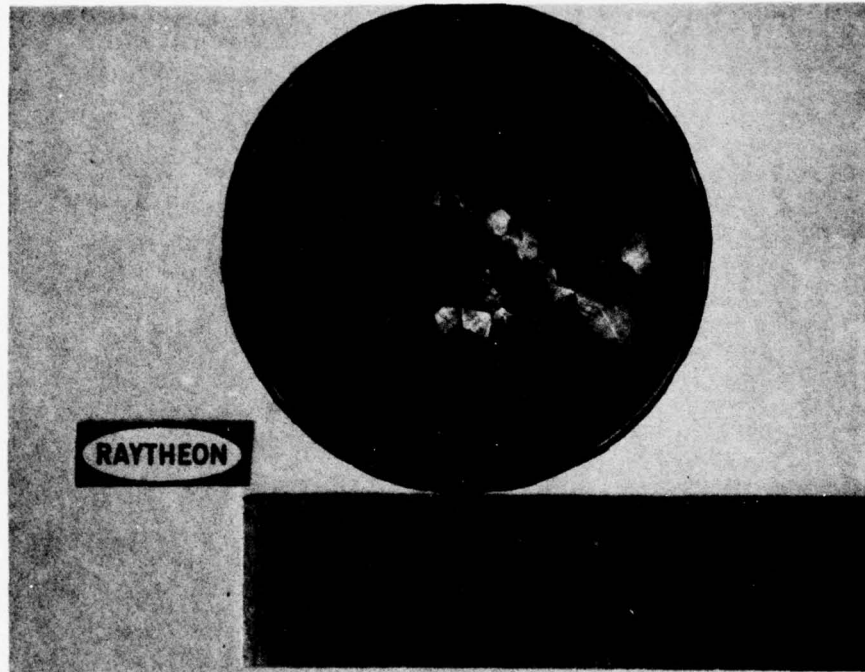


Figure 12. Fusion Cast Spinel Disc Photographed Between Crossed Polarizers to Reveal the Grain Structure (Same sample as shown in Figure 11.)

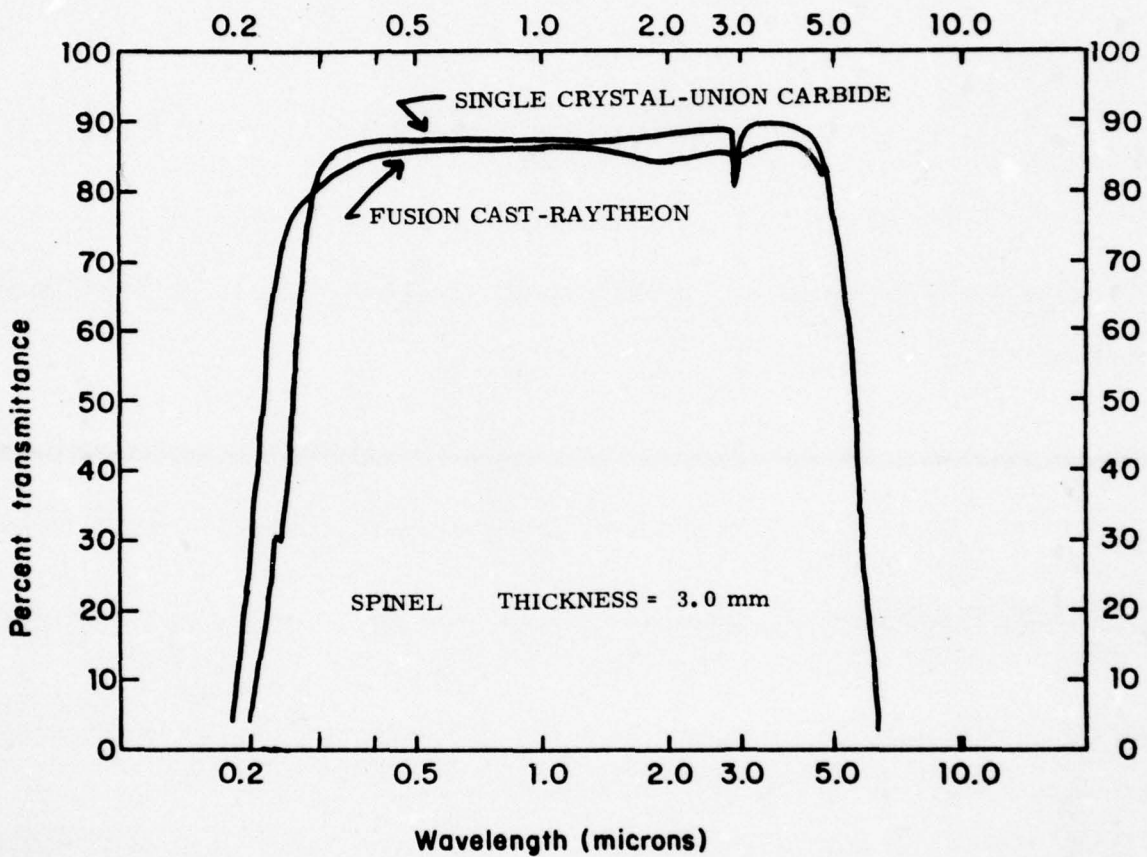


Figure 13. Optical Transmission Spectra of Fusion Cast and Single Crystal Spinel Samples (uncorrected for reflection losses).

multiphonon absorption near  $5 \mu\text{m}$  in the infrared. The only significant absorption band occurs at approximately  $3 \mu\text{m}$  and is likely due to "OH" impurities. This absorption is much less pronounced in the fusion cast spinel than in the single crystal material.

The fact that the transmittance does not drop off at visible wavelengths is a good indication of the absence of residual porosity which would cause optical scattering. Submicron size porosity would have little effect on transmittance at the longer infrared wavelengths, but as the wavelength becomes smaller and of the same size as the pores, even a minute amount of porosity will cause considerable optical scatter and consequent loss of transmittance.

A limited number of flexural strength and hardness measurements have been made on the fusion cast material. Strengths averaging about  $175 \text{ MN/m}^2$  (26,000 psi) have been measured in three-point loading. Knoop hardness ranges between 1700-1800  $\text{kg/mm}^2$  using a 200 gram load.

#### 4.3 Current Status and Plans

Problems with reproducibility of totally defect-free castings are currently being addressed. The critical parameter appears to be the shape and movement of the solid-liquid interface. Ideally a planar interface moves slowly and uniformly upperward through the mold as the furnace temperature is slowly decreased. To date, however, it has been difficult to achieve this ideal behavior reproducibly.

More typically, the interface appears to be planar at the start of solidification but then tends to become spiked or dendritic. This results in the bottom portion of the casting being totally clear while in the upper regions there are voids at grain boundaries.

To maintain a planar interface, increased temperature gradients and slower cooling rates are being investigated within the limitations of the

present system. Specifically, the necessity of melting the entire charge limits the magnitude of the gradient as a practical matter. Furthermore, it is difficult to impose a gradient upon a basically transparent material at high temperature where radiation is the dominant mechanism of heat transfer. There is also a minimum practical cooling rate in the present system due to the indirect regulation of the temperature by means of controlling furnace power.

After the flat plate casting process has been perfected, a stock of flat discs of alumina-rich spinel will be fabrication for subsequent hot forging into dome shapes.

## 5.0 HOT FORGING OF SPINEL

The basic feasibility of fabricating alumina-rich spinel shapes by hot forging was demonstrated. A number of rectangular beams were deformed in three-point loading at about 1750° C.

Beams of polycrystalline spinel with 2:1 molar ratio of  $\text{Al}_2\text{O}_3$  to  $\text{MgO}$  and 3.4:1 single crystal spinel were used. Dimensions of the samples were lengths of 25.4 to 38.1 mm, widths of 4.7 to 8.5 mm, and thicknesses of 2.4 to 3.2 mm. They were set in graphite fixtures so that spans of 20.6 or 25.4 mm could be loaded at the center point by weights suspended below the furnace (Figure 14). A graphite heating element provided temperatures to 1600° C to 1820° C in an atmosphere of helium. The applied loads produced maximum stresses in the sample beams of 19.2 to 70.3  $\text{MN/m}^2$  (2780 to 10,190 psi).

Deflection of the beams was monitored during each run. Data are presented in Table 5 and Figures 15 and 16. In Figure 17, some of the deformed beams are shown with a mm rule for scale. It is seen that some beams were bent to a 90 degree angle.

Deflection rates appear to be more sensitive to temperature than to stress level. There appears to be little difference in deformation behavior between the 3.4:1 single crystal and 2:1 polycrystalline materials. This is in keeping with findings presented by Mitchell et al.<sup>1</sup> in their work on compressive deformation of spinel. They found a significant difference between stoichiometric (1:1) and  $\text{Al}_2\text{O}_3$ -rich spinel but small variation between 2:1 and 3.5:1 spinels.

Surface degradation of the spinel material during these deformation experiments has been observed. The samples lost weight and a translucent "skin" resulted. However, the interior of the test beams was not affected.

<sup>1</sup>J. Mater. Science 11 (1976) 264.

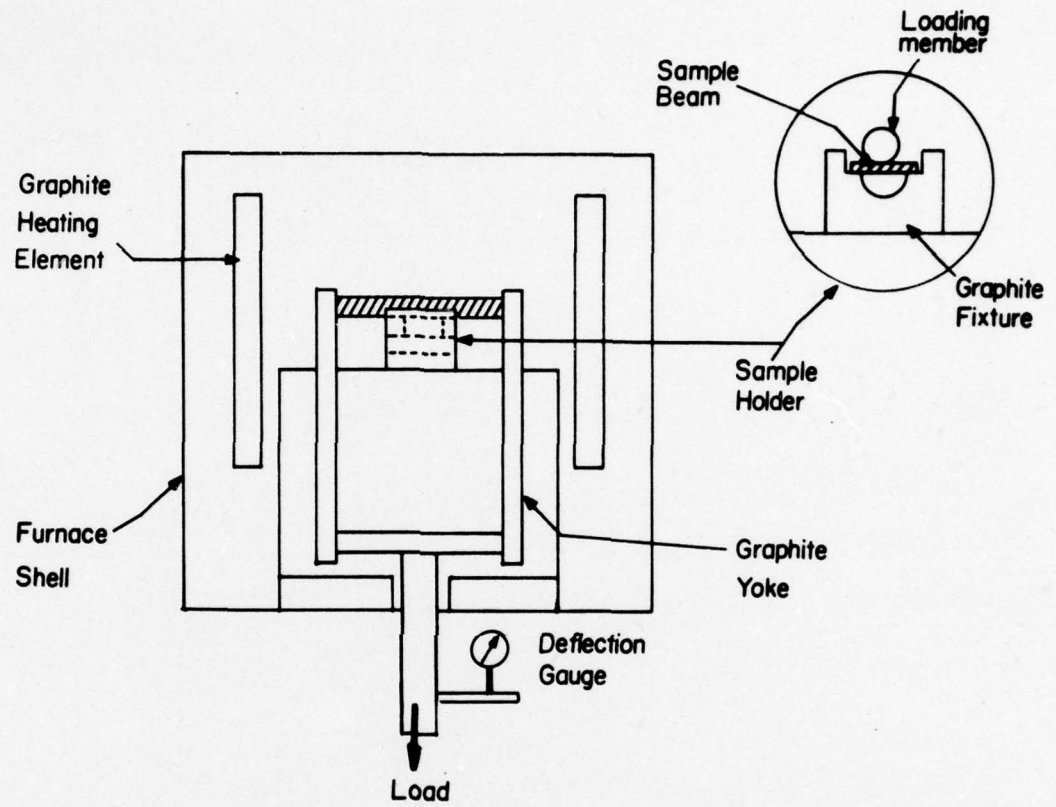


Figure 14. Apparatus for Three-Point Loading of Spinel Beams.

TABLE 5

BEAM DEFLECTION RUNS

<u>Material</u>	<u>Sample Code</u>	<u>Cross-Section (mm)</u>	<u>Span (mm)</u>	<u>Temp (° C)</u>	<u>Stress (MN/m<sup>2</sup>) (psi)</u>	<u>Max. Deflection (mm)</u>	<u>Deflection Rate (mm/hr)</u>	<u>Weight Loss (%)</u>
2:1 poly	24630-74	2.5 x 8.5	25.4	1820	50.2 7270	10.2	1.2-20.5	21.3
2:1 poly	24630-75	3.2 x 6.4	25.4	1755	40.2 5820	7.1	0.7-6.0	16.4
3.4:1 s. c.	24630-100	2.5 x 4.7	20.6	1750	38.4 5570	2.0	---	14.0
3.4:1 s. c.	24682-2	2.5 x 4.7	20.6	1750	51.2 7420	1.3	0.1-0.6	41.8
3.4:1 s. c.	24682-4	2.5 x 4.7	20.6	1780	55.2 8000	6.6	1.5-3.4	13.3
3.4:1 s. c.	24682-6	2.5 x 4.7	20.6	1760	27.2-53.6 3945-7765	8.5	0.2-4.2	21.6
3.4:1 s. c.	24682-7-2	2.5 x 5.0	20.6	1750	47.8-65.6 6935-9510	2.6	0.5-1.0	1.3
3.4:1 s. c.	24682-10	2.4 x 5.1	20.6	1745	51.6 7480	6.6	1.9-8.8	6.9

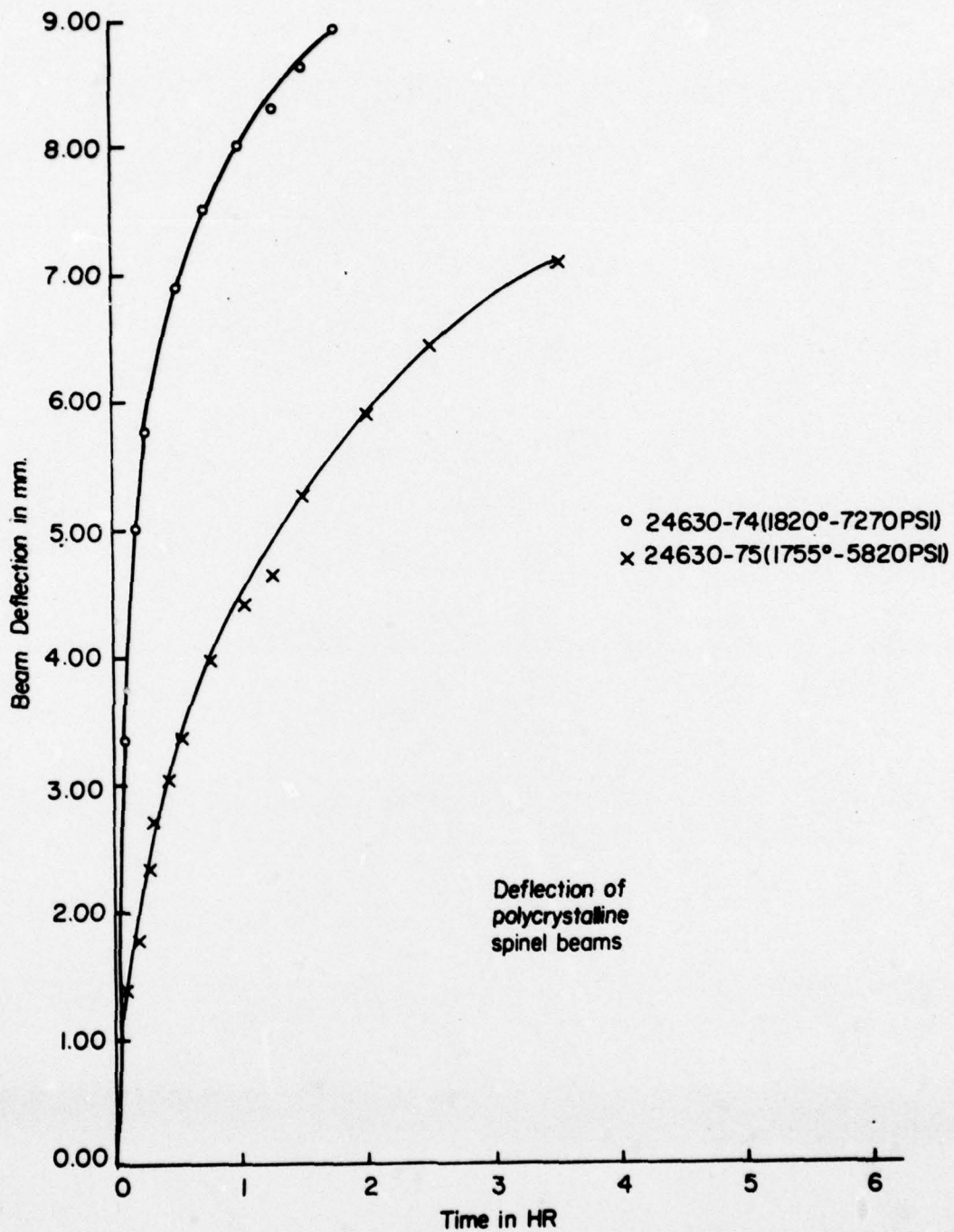


Figure 15. Deflection Vs Time for Polycrystalline 2:1 Spinel Beams

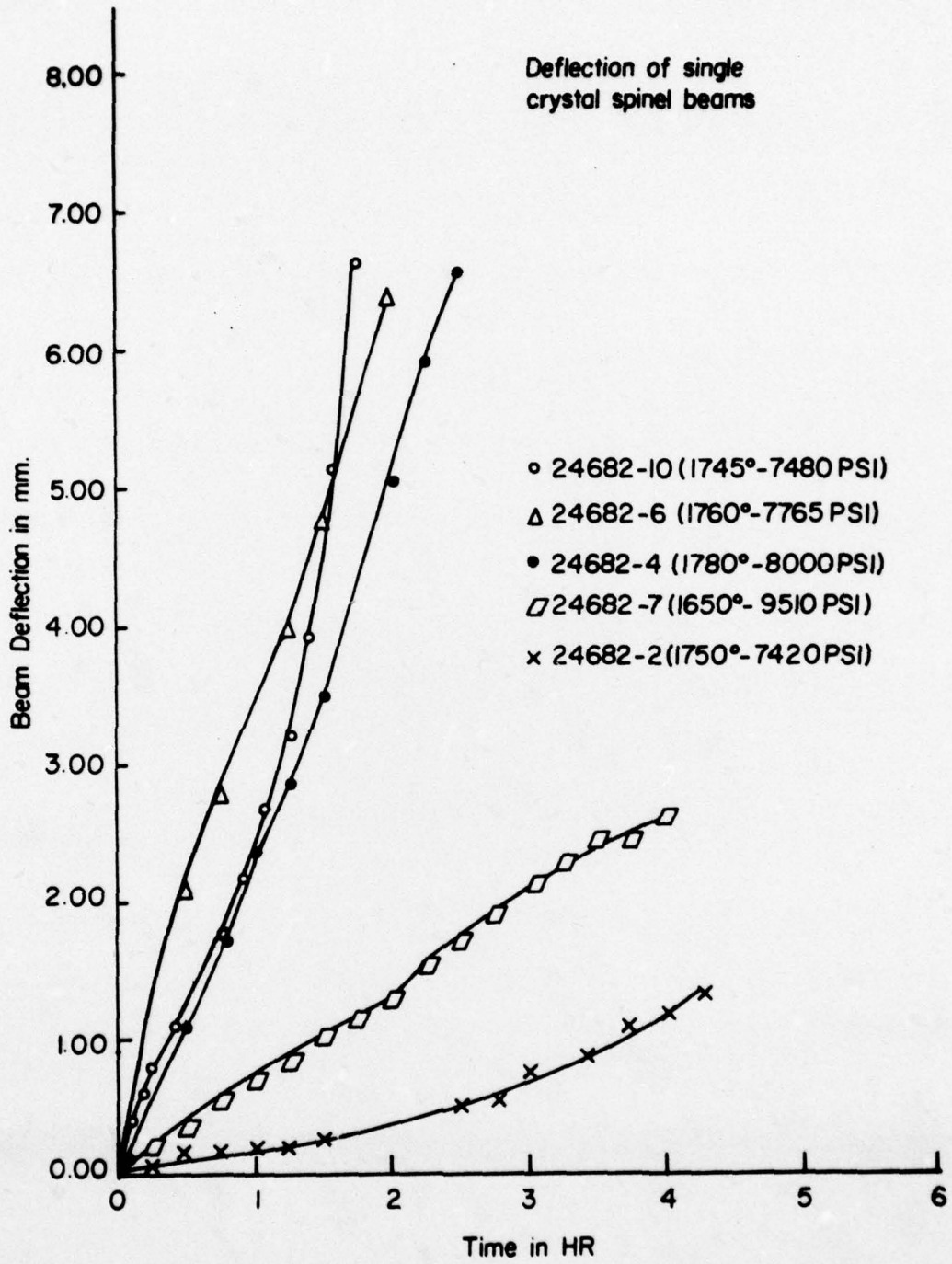


Figure 16. Deflection Vs Time for 3. 4:1 Single Crystal Spinel Beams

PBN-77-719

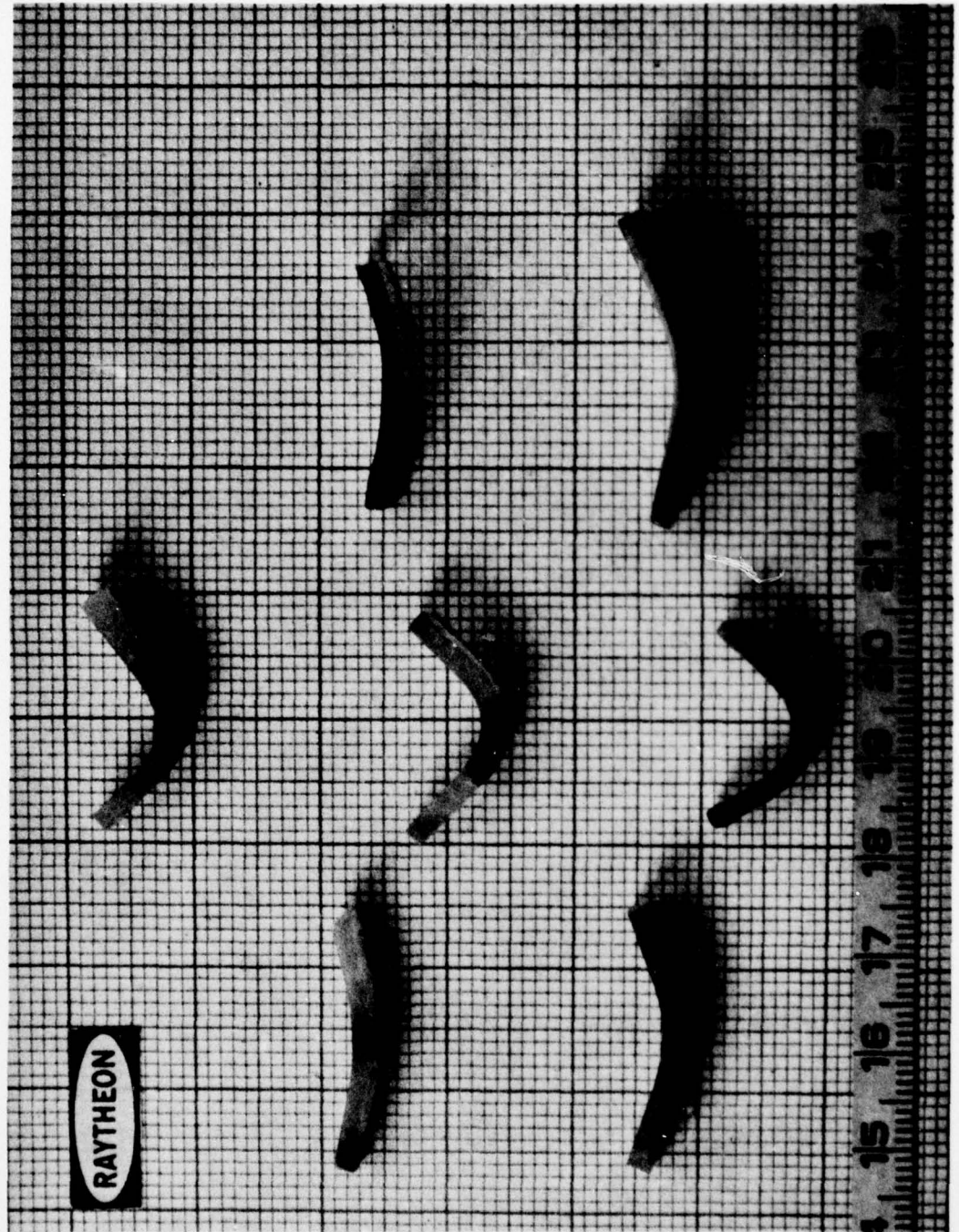


Figure 17. Deformed Beams of Alumina-Rich Spinel.  
Left and Center: Single Crystal  
Right: Polycrystalline

Attempts were made to isolate the beams from the graphite fixtures with separators of molybdenum and/or tantalum foil. These were not particularly successful. In fact, 0.4 mm thick Grafoil (Fiber Materials Inc.) used in the same manner seemed to protect the beam better. Data on weight loss during the various deflection runs is included in Table 5.

Future work on forging of spinel is planned in which fusion cast flat plates will be deformed between male and female hemispherical mandrels to form dome shapes.

<u>Organization</u>	<u>No. of Copies</u>	<u>Organization</u>	<u>No. of Copies</u>
Defense Documentation Center Cameron Station Alexandria, Virginia 22314	(12)	Naval Construction Battalion Civil Engineering Laboratory Port Hueneme, California 93043 Attn: Materials Division	(1)
Office of Naval Research Department of the Navy  Attn: Code 471 Code 102 Code 470	(1) (1) (1)	Naval Electronics Laboratory Center San Diego, California 92152 Attn: Electron Materials Sciences Division	(1)
Commanding Officer Office of Naval Research Branch Office 495 Summer Street Boston, Massachusetts 02210	(1)	Naval Missile Center Materials Consultant Code 3312-1 Point Mugu, California 93041	(1)
Commanding Officer Office of Naval Research Branch Office 536 South Clark Street Chicago, Illinois 60605	(1)	Commanding Officer Naval Surface Weapons Center White Oak Laboratory Silver Spring, Maryland 20910 Attn: Library	(1)
Office of Naval Research San Francisco Area Office 760 Market Street, Room 447 San Francisco, California 94102 Attn: Dr. P. A. Miller	(1)	David W. Taylor Naval Ship R&D Center Materials Department Annapolis, Maryland 21402	(1)
Naval Research Laboratory Washington, D.C. 20390  Attn: Code 6000 Code 6100 Code 6300 Code 6400 Code 2627	(1) (1) (1) (1) (1)	Naval Undersea Center San Diego, California 92132 Attn: Library	(1)
Naval Air Development Center Code 302 Warminster, Pennsylvania 18974 Attn: Mr. F. S. Williams	(1)	Naval Underwater System Center Newport, Rhode Island 02840 Attn: Library	(1)
Naval Air Propulsion Test Center Trenton, New Jersey 08628 Attn: Library	(1)	Naval Weapons Center China Lake, California 93555 Attn: Library	(1)
		Naval Postgraduate School Monterey, California 93940 Attn: Mechanical Engineering Dept.	(1)
		Naval Air Systems Command Washington, D.C. 20360  Attn: Code 52031 Code 52032 Code 320	(1) (1) (1)

<u>Organization</u>	<u>No. of Copies</u>	<u>Organization</u>	<u>No. of Copies</u>
Naval Sea System Command Washington, D.C. 20362 Attn: Code 035	(1)	NASA Headquarters Washington, D.C. 20546 Attn: Code RRM	(1)
Naval Facilities Engineering Command Alexandria, Virginia 22331 Attn: Code 03	(1)	NASA Lewis Research Center 21000 Brookpark Road Cleveland, Ohio 44135 Attn: Library	(1)
Scientific Advisor Commandant of the Marine Corps Washington, D.C. 20380 Attn: Code AX	(1)	National Bureau of Standards Washington, D.C. 20234  Attn: Metallurgy Division (1) Inorganic Materials Division (1)	
Naval Ship Engineering Center Department of the Navy CTR BG #2 3700 East-West Highway Prince Georges Plaza Hyattsville, Maryland 20782 Attn: Engineering Materials and Services Office, Code 6101	(1)	Defense Metals and Ceramics Information Center Battelle Memorial Institute 505 King Avenue Columbus, Ohio 43201	(1)
Army Research Office Box CM, Duke Station Durham, North Carolina 27706 Attn: Metallurgy & Ceramics Div.	(1)	Director Ordnance Research Laboratory P.O. Box 30 State College, Pennsylvania 16801	(1)
Army Materials and Mechanics Research Center Watertown, Massachusetts 02172 Attn: Res. Programs Office (AMXMR-P)	(1)	Director Applied Physics Laboratory University of Washington 1013 Northeast Fortieth Street Seattle, Washington 98105	(1)
Air Force Office of Scientific Research Bldg. 410 Bolling Air Force Base Washington, D.C. 20332 Attn: Chemical Science Directorate (1) Electronics and Solid State Sciences Directorate (1)		Metals and Ceramics Division Oak Ridge National Laboratory P.O. Box X Oak Ridge, Tennessee 37380	(1)
Air Force Materials Lab (LA) Wright-Patterson AFB Dayton, Ohio 45433	(1)	Los Alamos Scientific Laboratory P.O. Box 1663 Los Alamos, New Mexico 87544 Attn: Report Librarian	(1)
		Argonne National Laboratory Metallurgy Division P.O. Box 229 Lemont, Illinois 60439	(1)

<u>Organization</u>	<u>No. of Copies</u>	<u>Organization</u>	<u>No. of Copies</u>
Brookhaven National Laboratory Technical Information Division Upton, Long Island New York 11973 Attn: Research Library	(1)		
Library Building 50 Room 134 Lawrence Radiation Laboratory Berkeley, California	(1)		

<u>Organization</u>	<u>No. of Copies</u>	<u>Organization</u>	<u>No. of Copies</u>
Dr. W.F. Adler Effects Technology Inc. 5383 Hollister Avenue P.O. Box 30400 Santa Barbara, CA 92105	(1)	Professor A.H. Heuer Case Western Reserve University University Circle Cleveland, OH 44106	(1)
Dr. G. Bansal Battelle 505 King Avenue Columbus, OH 43201	(1)	Dr. R. Hoagland Battelle 505 King Avenue Columbus, OH 43201	(1)
Dr. R. Bratton Westinghouse Research Lab. Pittsburgh, PA 15235	(1)	Dr. R. Jaffee Electric Power Research Institute Palo Alto, CA	(1)
Dr. A.G. Evans Rockwell International P.O. Box 1085 1049 Camino Dos Rios Thousand Oaks, CA 91360	(1)	Dr. P. Jorgensen Stanford Research Institute Poulter Laboratory Menlo Park, CA 94025	(1)
Mr. E. Fisher Ford Motor Co. Dearborn, MI	(1)	Dr. R.N. Katz Army Materials and Mechanics Research Center Watertown, MA 02171	(1)
Dr. P. Gielisse University of Rhode Island Kingston, RI 02881	(1)	Dr. H. Kirchner Ceramic Finishing Company P.O. Box 498 State College, PA 16801	(1)
Dr. M.E. Gulden International Harvester Company Solar Division 2200 Pacific Highway San Diego, CA 92138	(1)	Dr. B. Koepke Honeywell, Inc. Corporate Research Center 500 Washington Avenue, South Hopkins, MN 55343	(1)
Dr. D.P.H. Hasselman Montana Energy and MHD Research and Development Institute P.O. Box 3809 Butte, Montana 59701	(1)	Mr. Frank Koubek Naval Surface Weapons Center White Oak Laboratory Silver Spring, MD 20910	(1)
Mr. G. Hayes Naval Weapons Center China Lake, CA 93555	(1)	E. Krafft Carborundum Co. Niagara Falls, NY	(1)

<u>Organization</u>	<u>No. of Copies</u>	<u>Organization</u>	<u>No. of Copies</u>
Dr. F.F. Lange Rockwell International P.O. Box 1085 1049 Camino Dos Rios Thousand Oaks, CA 91360	(1)	Dr. J. Ritter University of Massachusetts Department of Mechanical Engineering Amherst, MA 01002	(1)
Dr. J. Lankford Southwest Research Institute 8500 Culebra Road San Antonio, TX 78284	(1)	Professor R. Roy Pennsylvania State University Materials Research Laboratory University Park, PA 16802	(1)
Library Norton Company Industrial Ceramics Division Worcester, MA 01606	(1)	Dr. R. Ruh AFML Wright-Patterson AFB Dayton, OH 45433	(1)
State University of New York College of Ceramics at Alfred University Attn: Library Alfred, NY 14802	(1)	Mr. J. Schuldies AiResearch Phoenix, AZ	(1)
Dr. L. Hench University of Florida Ceramics Division Gainesville, FL 32601	(1)	Professor G. Sines University of California, Los Angeles Los Angeles, CA 90024	(1)
Dr. N. MacMillan Materials Research Laboratory Pennsylvania State University College Park, PA 16802	(1)	Dr. N. Tallan AFML Wright-Patterson AFB Dayton, OH 45433	(1)
Mr. F. Markarian Naval Weapons Center China Lake, CA 93555	(1)	Dr. T. Vasilos AVCO Corporation Research and Advanced Development Division 201 Lowell Street Wilmington, MA 01887	(1)
Dr. Perry A. Miles Raytheon Company Research Division 28 Seyon Street Waltham, MA 02154	(1)	Mr. J.D. Walton Engineering Experiment Station Georgia Institute of Technology Atlanta, GA 30332	(1)
Mr. R. Rice Naval Research Laboratory Code 6360 Washington, D.C. 20375	(1)	Dr. S.M. Widerhorn Inorganic Materials Division National Bureau of Standards Washington, DC 20234	(1)

<u>Organization</u>	<u>No. of Copies</u>	<u>Organization</u>	<u>No. of Copies</u>
Dr. S.A. Bortz IITRI 10 W. 35th Street Chicago, IL 60616	(1)	Major W. Simmons Air Force Office of Scientific Research Building 410 Bolling Air Force Base Washington, DC 20332	(1)
Mr. G. Schmitt Air Force Materials Laboratory Wright-Patterson AFB Dayton, OH 45433	(1)	Dr. P. Becher Naval Research Laboratory Code 6362 Washington, DC 20375	(1)
Dr. D.A. Shockey Stanford Research Institute Poulter Laboratory Menlo Park, CA 94025	(1)	Mr. L.B. Weckesser Applied Physics Laboratory Johns Hopkins Road Laurel, MD 20810	(1)
Dr. W.G.D. Frederick Air Force Materials Laboratory Wright-Patterson AFB Dayton, OH 45433	(1)	Mr. D. Richarson AiResearch Manufacturing Company 4023 36th Street P.O. Box 5217 Phoenix, AZ 85010	(1)
Dr. P. Land Air Force Materials Laboratory Wright-Patterson AFB Dayton, OH 45433	(1)	Dr. H.E. Bennett Naval Weapons Center Code 3818 China Lake, CA 93555	(1)
Mr. K. Letson Redstone Arsenal Huntsville, AL 35809	(1)	Mr. G. Denman Air Force Materials Laboratory Code LPJ Wright-Patterson AFB Dayton, OH 45433	(1)
Dr. S. Freiman Naval Research Laboratory Code 6363 Washington, DC 20375	(1)	Dr. D. Godfrey Admiralty Materials Laboratory Polle, Dorset BH16 6JU UNITED KINGDOM	(1)
Director Materials Sciences Defense Advanced Research Projects Agency 1400 Wilson Boulevard Arlington, VA 22209	(1)	Dr. N. Corney Ministry of Defense The Adelphi John Adam Street London WC2N 6BB UNITED KINGDOM	(1)
Dr. James Pappis Raytheon Company Research Division 28 Seyon Street Waltham, MA 02154	(1)		

<u>Organization</u>	<u>No. of Copies</u>	<u>Organization</u>	<u>No. of Copies</u>
Dr. L.M. Gillin Aeronautical Research Laboratory P.O. Box 4331 Fisherman's Bend Melbourne, VIC 3001 AUSTRALIA	(1)		